

Article

Numerical Simulation of Proppant Transport in Transverse Fractures of Horizontal Wells

Zhengrong Chen ¹, Xin Xie ¹, Guangai Wu ^{1,*}, Yanan Hou ¹, Bumin Guo ² and Yantao Xu ²

¹ CNOOC Research Institute Ltd., Beijing 100028, China; chenrzcnooc@163.com (Z.C.); xiexin3@cnooc.com.cn (X.X.); houyn2@cnooc.com.cn (Y.H.)

² Oilfield Production Research Institute of COSL, Tianjin 300459, China; baitaocnooc@163.com (B.G.); xuyt4@cosl.com.cn (Y.X.)

* Correspondence: wgai_cnooc@126.com

Abstract: Proppant transport and distribution law in hydraulic fractures has important theoretical and field guidance significance for the optimization design of hydraulic fracturing schemes and accurate production prediction. Many studies aim to understand proppant transportation in complex fracture systems. Few studies, however, have addressed the flow path mechanism between the transverse fracture and horizontal well, which is often neglected in practical design. In this paper, a series of mathematical equations, including the rock elastic deformation equation, fracturing fluid continuity equation, fracturing fluid flow equation, and proppant continuity equation for the proppant transport, were established for the transverse fracture of a horizontal well, while the finite element method was used for the solution. Moreover, the two-dimensional radial flow was considered in the proppant transport modeling. The results show that proppant breakage, embedding, and particle migration are harmful to fracture conductivity. The proppant concentration and fracture wall roughness effect can slow down the proppant settling rate, but at the same time, it can also block the horizontal transportation of the proppant and shorten the effective proppant seam length. Increasing the fracturing fluid viscosity and construction displacement, reducing the proppant density and particle size, and adopting appropriate sanding procedures can all lead to better proppant placement and, thus, better fracturing and remodeling results. This paper can serve as a reference for the future study of proppant design for horizontal wells.



Citation: Chen, Z.; Xie, X.; Wu, G.; Hou, Y.; Guo, B.; Xu, Y. Numerical Simulation of Proppant Transport in Transverse Fractures of Horizontal Wells. *Processes* **2024**, *12*, 909. <https://doi.org/10.3390/pr12050909>

Academic Editors: Xian Shi and Qingbang Meng

Received: 19 February 2024

Revised: 3 April 2024

Accepted: 22 April 2024

Published: 29 April 2024



Copyright: © 2024 by the authors. Licensee MDPI, Basel, Switzerland. This article is an open access article distributed under the terms and conditions of the Creative Commons Attribution (CC BY) license (<https://creativecommons.org/licenses/by/4.0/>).

Keywords: proppant transportation; hydraulic fracturing; transverse fracture; numerical simulation; horizontal well

1. Introduction

In recent years, a series of breakthroughs have been made in the exploration and development of unconventional oil and gas worldwide, and the production of unconventional oil and gas is growing rapidly and becoming increasingly prominent in the global energy supply. The application of the hydraulic fracturing technique on horizontal wells has been successfully applied in the unlocking of unconventional reservoirs, and the final hydraulic fracturing effectiveness has a close relationship with the proppant distributions [1–4]. Due to the fact that horizontal wells are usually drilled along the direction of the minimum horizontal principal stress, multiple transverse fractures can be generally created. The connection between the transverse fracture and horizontal wellbore can result in special flow conditions, thus affecting the proppant flow into fractures. Thus, understanding the proppant transport along the transverse fractures of horizontal wells is necessary.

Due to uncertainty in the hydraulic fracture, the proppant design remains a great challenge in the oil and gas industry. Some authors have previously used numerical and experimental methods in this research area to better understand the proppant movement in hydraulic fractures. Sahai et al., 2014 investigated the proppant transport in complex hydraulic fractures, and they found the proppant size, density, and pump rate all had

an impact on proppant transport [5]. Wang et al., 2019 analyzed the influences of injection time, injection rate, fracturing fluid viscosity, and proppant combination type on the migration and sedimentation law of a proppant in single and branch fractures. They demonstrated that when the fracture morphology is single, the viscosity of the fracturing fluid is recommended to be between 30 and 60 mPa·s. When the fracture morphology is complex, the recommended value is between 40 and 50 mPa·s [6]. Wang et al., 2020 focused on modeling and examining proppant movement with respect to the diversion of energy. The experimental results indicate that proppant breakage, embedding, and particle migration are harmful to fracture conductivity. With the increase in closure pressure to 50 MPa, large embedding of the proppant occurs, and damage to the conductivity increases from 12.7% to 85.6% [7]. Suri et al., 2020 studied the effect of fracture roughness on proppant transport in hydraulic fractures using the Joint Roughness Coefficient and a three-dimensional multiphase modeling approach. They believed that the interproppant and proppant wall interactions become dominant, which adds turbulence to the flow [8]. Merzoug et al., 2022 discussed proppant placement efficiency considering the hydraulic fracture and natural fracture interaction. They revealed that the effect of the pre-existing fracture friction angle and the angle of approach, as well as the differential horizontal stress on hydraulic fracture and natural fracture interaction mechanisms and proppant transport and placement [9]. Zheng et al., 2023 introduced a CFD (Computational Fluid Dynamics)-DEM (Discrete Element Method) technique to investigate the effects of different roughness characterization parameters on the efficiency of proppant transport using supercritical CO₂. They suggested higher pump power is required for efficient proppant transport using supercritical CO₂; otherwise, sand plugs may occur [10]. Although various experimental and numerical research studies have been performed on proppant transport at vertical or horizontal wellbores, the proppant transport process at transverse fractures has rarely been reported in the literature. In particular, the flow pattern of the fracturing fluid and the proppant delivery law in transverse fractures in horizontal wells differ significantly from that of conventional hydraulic fracturing [11–15]. In recent years, some authors have tended to consider more complex fracture conditions, such as fracture surface roughness. Through the reconstruction of rock surfaces using 3D techniques, the comparison between the proppant transport behavior for the smooth and rough fractures can be discussed. In addition, under this condition, the fracturing fluid velocity and viscosity and particle density and size can be investigated. In previous studies, numerical simulation research was mainly performed to understand the proppant transport mechanism in hydraulic fractures. Moreover, the CFD-DEM method has been commonly used in the field of proppant transport, and its validated effectiveness has been recognized. However, when the fracture geometry is complex, such as in secondary branch fracture development, the computational load for the proppant transport is heavy and cannot be applied for the field application. Considering multiphase flow simulation and the coupling between proppant transport and crack propagation, numerical modeling is more complex [16–21]. The radial flow zones around the wellbore of horizontal wells can be observed, while the two-dimensional flow of the fracturing fluid should be considered. Furthermore, proppant transportation in horizontal wells is rarely studied [22–24]. To offset the calculation efficiency, the analytical modeling of proppant transportation is necessary.

Thus, in this study, a coupled proppant transportation equation is used to simulate the proppant transport process in transverse fractures of horizontal wells. Field data are used to verify the accuracy of this model. Several numerical simulations are carried out under different conditions to study the proppant transport process and determine the critical factors of proppant distribution. These studies can provide a better understanding of the proppant transport process in transverse fractures of horizontal wells, which is helpful to the proppant schedule design.

2. Model Establishment

Horizontal wells are generally oriented along the direction of the minimum horizontal ground stress; thus, horizontal well fracturing usually forms transverse fractures perpendicular to the axis of the wellbore. Regardless of the fracture geometry model adopted and the fracture morphology, due to the unique internal boundary conditions, there exists a region of a radial flow of fracturing fluid near the wellbore, which is a distinctive feature of fracturing fluid flow within the transverse fracture of horizontal well fracturing. This fracturing fluid flow characteristic can have an impact on the fracture morphology and proppant delivery, and, at the same time, due to the presence of the radial flow field, it may increase the complexity of fractures in the near-wellbore zone and generate additional friction; thus, there is a high risk of sand plugging when sand-carrying fluids are flowing in it. The hydraulic fracturing model usually consists of three basic control equations, which are the mass conservation equation of the injected fluid, the rock fracture mechanics equation that relates the fracture width to the fluid pressure distribution inside the fracture, and the fluid flow equation that describes the pressure and fluid flow inside the fracture. These are the basic equations for describing and controlling the hydraulic fracturing process, and the dynamics of the fracture can be obtained by the coupling of the three equations. The dynamic fracture expansion process can be obtained by solving the coupled solution of the above three equations. In addition, in order to describe the loss of fracturing fluid into the formation during the fracturing process, the transportation of proppant, and the distribution of the temperature field in the fracture and the formation, the hydraulic fracturing model should also include the equation for the loss of fracturing fluid filtration, the equation for the transportation of proppant, and the equation for calculating the temperature field, etc. The model should also include the equations of fracturing fluid filtration, proppant transportation, and temperature field calculation, as shown in Figure 1.

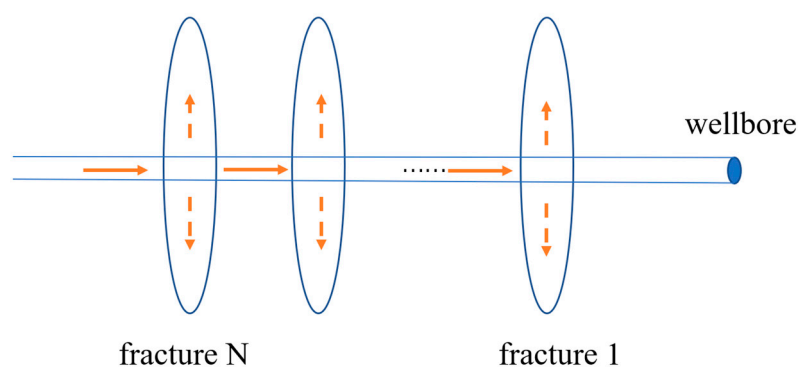


Figure 1. Schematic diagram of multiple transverse fractures in a horizontal well.

2.1. Assumptions

To accurately characterize the proppant transport along the transverse fracture of a horizontal well, the modeling of proppant transport should follow several assumptions.

- (1) The formation rocks are linear elastomers, and fracture cracking and expansion satisfy linear elastic fracture mechanics;
- (2) A single shot hole cluster can be simplified as an annular cut in the wellbore wall, and the hydraulic fracture initiates radially at this annular cut;
- (3) The fracture height is well controlled by the spacer, and the fracture extends only within the reservoir;
- (4) The fracturing fluid is an incompressible Newtonian fluid, which flows in a two-dimensional laminar flow in the fracture;
- (5) The flow of fracturing fluid in the fracture is between two parallel walls, and the influence of gravity on the flow of fracturing fluid is not considered;
- (6) The rate of loss of fracturing fluid at a point in the fracture depends on the time that the point is exposed to the fracturing fluid and satisfies the Carter loss equation, but

the loss of fracturing fluid from the formation does not affect the fluid pressure distribution in the fracture;

(7) The velocity gradient of the fracturing fluid in the fracture length and fracture height directions is negligible compared to the velocity gradient of the fracturing fluid across the width of the fracture;

(8) The effect of temperature field changes within the fracture on the rheology of the fracturing fluid is not considered.

The basic axis system can be illustrated, as shown in Figure 2, and the related boundary condition can be set. The fracture height is equal to the pay zone thickness due to stress confinement between the pay zone and the boundary zone; thus, two-dimensional flow in the x-axis and y-axis can be assumed.

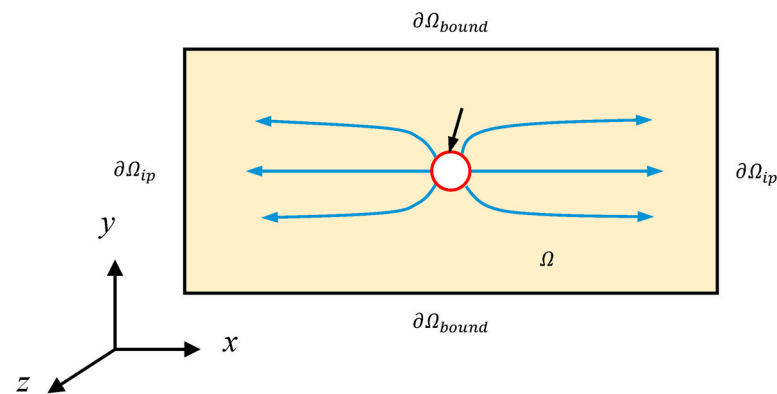


Figure 2. Model computation domain and coordinate system. The black arrow represents the wellbore; The blue arrow represents the direction of proppant transport.

2.2. Continuity Equations

In the vicinity of the wellbore, there exists a region of a radial flow of fracturing fluid, whose flow direction can be decomposed into two components, horizontal and vertical. Thus, in the following model derivation process, the two-dimensional continuity equations and differential equations of motion of the fracturing fluid in the x–y planes are established and combined with the boundary conditions and the initial conditions to determine the distribution of the flow field inside the fracture. Figure 3 illustrates the control body unit of a hydraulic fracture. Any one control body unit inside the fracture is selected as the study object, and its length, height, and width are dx , dy , and dz , respectively.

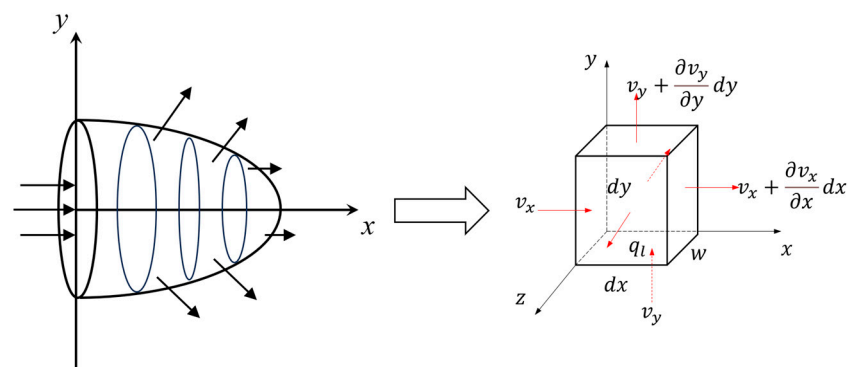


Figure 3. Control body unit of hydraulic fracture. Arrows represent the direction of seepage.

According to the law of the conservation of mass, the reduction in the mass of the control body at time dt must be equal to the difference between the outgoing and incoming masses:

$$\frac{\partial(\rho_s v_x w)}{\partial x} dx dy dt + \frac{\partial(\rho_s v_y w)}{\partial y} dx dy dt + 2\rho_f v_l dx dy dt = -\frac{\partial(\rho_s w)}{\partial t} dx dy dt \quad (1)$$

The continuity equation for the sand-carrying fluid is:

$$\frac{\partial(\rho_s(x, y, t)w(x, y, t))}{\partial t} + \nabla \cdot (\rho_s(x, y, t)\mathbf{q}(x, y, t)) + 2\rho_f v_l(x, y, t) = 0 \quad (2)$$

In this formula, ρ_s is the density of the sand-carrying liquid, kg/m^3 ; ρ_f is the density of the pure fracturing fluid, kg/m^3 ; v_x is the flow rate of fracturing fluid along the x -axis, m/s ; v_y is the flow rate of fracturing fluid along the y -axis, m/s ; v_l is the filtration velocity of fracturing fluid along the z -axis to the formation, m/s ; q_x is the flow rate per unit fracture height in the x -direction, m^3/s ; q_y is the flow rate per unit fracture length in the y -direction, m ; and w is the crack width, m .

The density of the sand-carrying liquid can be calculated by the following formula:

$$\rho_s = c\rho_p + (1 - c)\rho_f \quad (3)$$

In this formula, ρ_p is the density of proppant, kg/m^3 ; and c is the proppant volume concentration, decimal.

The continuity equation of pure fracturing fluid is:

$$\frac{\partial w(x, y, t)}{\partial t} + \nabla \cdot \mathbf{q}(x, y, t) = -2v_l(x, y, t) \quad (4)$$

The filtration velocity of the carrier fluid can be calculated by the Cater filtration equation:

$$v_l = \frac{C_t}{\sqrt{t - \tau}} \quad (5)$$

In the equation, C_t is the overall filtrate coefficient for the liquid, $\text{m}/\sqrt{\text{s}}$; t is the hydraulic fracturing duration, s ; and τ is the time at which filtrate begins at a certain point in the fracture, s .

The overall filtrate coefficient is calculated as follows:

$$\frac{1}{C_t} = \frac{1}{C_1} + \frac{1}{C_2} + \frac{1}{C_3} \quad (6)$$

During the hydraulic fracturing process, a portion of the injected fracturing fluid from the surface is used to expand the volume of the fractures, while another portion is lost or filtrates into the formation. Therefore, the total mass conservation equation for the fracturing fluid is as follows:

$$-\int_{\Omega} \int_0^t 2v_l dx dy dt - \int_{\Omega} \int_0^t \frac{\partial w}{\partial t} dx dy dt + \int_0^t Q_i dt = 0 \quad (7)$$

In the Q_i equation, represents the injection rate of the fracturing fluid at the wellbore perforation site, m^3/s .

2.3. Fluid Flow Equation

Navier–Stokes equations are basic equations describing the flow of viscous fluids. Assuming that the fracture width is very small compared to the scales of the fracture length and height and that the fracture width changes uniformly and smoothly, the three-dimensional Navier–Stokes equations can be simplified to two-dimensional equations,

which, in turn, lead to the so-called lubrication equations or the so-called cubic law. The Navier–Stokes equations for three-dimensional flow are as follows:

$$\begin{cases} v_x \frac{\partial v_x}{\partial x} + v_y \frac{\partial v_x}{\partial y} + v_z \frac{\partial v_x}{\partial z} = -\frac{1}{\rho} \frac{\partial p}{\partial x} + \frac{\mu}{\rho} \left(\frac{\partial^2 v_x}{\partial x^2} + \frac{\partial^2 v_x}{\partial y^2} + \frac{\partial^2 v_x}{\partial z^2} \right) \\ v_x \frac{\partial v_y}{\partial x} + v_y \frac{\partial v_y}{\partial y} + v_z \frac{\partial v_y}{\partial z} = -\frac{1}{\rho} \frac{\partial p}{\partial y} + \frac{\mu}{\rho} \left(\frac{\partial^2 v_y}{\partial x^2} + \frac{\partial^2 v_y}{\partial y^2} + \frac{\partial^2 v_y}{\partial z^2} \right) \\ v_x \frac{\partial v_z}{\partial x} + v_y \frac{\partial v_z}{\partial y} + v_z \frac{\partial v_z}{\partial z} = -\frac{1}{\rho} \frac{\partial p}{\partial z} + \frac{\mu}{\rho} \left(\frac{\partial^2 v_z}{\partial x^2} + \frac{\partial^2 v_z}{\partial y^2} + \frac{\partial^2 v_z}{\partial z^2} \right) \end{cases} \quad (8)$$

Disregarding the flow of fracturing fluid along the width direction of the fracture, we have: $v_z = 0$. This results in the simplification of the aforementioned three-dimensional Navier–Stokes equations into a two-dimensional equation:

$$\begin{cases} v_x \frac{\partial v_x}{\partial x} + v_y \frac{\partial v_x}{\partial y} = -\frac{1}{\rho} \frac{\partial p}{\partial x} + \frac{\mu}{\rho} \left(\frac{\partial^2 v_x}{\partial x^2} + \frac{\partial^2 v_x}{\partial y^2} + \frac{\partial^2 v_x}{\partial z^2} \right) \\ v_x \frac{\partial v_y}{\partial x} + v_y \frac{\partial v_y}{\partial y} = -\frac{1}{\rho} \frac{\partial p}{\partial y} + \frac{\mu}{\rho} \left(\frac{\partial^2 v_y}{\partial x^2} + \frac{\partial^2 v_y}{\partial y^2} + \frac{\partial^2 v_y}{\partial z^2} \right) \end{cases} \quad (9)$$

By integrating Equation (9) with respect to z twice and substituting the boundary conditions from the equation, we obtain:

$$\begin{cases} v_x(z) = \frac{1}{2\mu} \left(z^2 - \frac{w^2}{4} \right) \frac{\partial p}{\partial x} \\ v_y(z) = \frac{1}{2\mu} \left(z^2 - \frac{w^2}{4} \right) \frac{\partial p}{\partial y} \end{cases} \quad (10)$$

Equation (11) represents the expressions of the velocity distributions of u and w in the z -direction. Integrating them separately with respect to z from $-\frac{w}{2}$ to $\frac{w}{2}$, we have the following description:

$$\begin{cases} q_x = -\frac{w^3}{12\mu} \frac{\partial p}{\partial x} \\ q_y = -\frac{w^3}{12\mu} \frac{\partial p}{\partial y} \end{cases} \quad (11)$$

Below expresses Equation (12) in vector form:

$$\nabla p(x, y, t) = -\frac{12\mu}{w^3(x, y, t)} q(x, y, t) \quad (12)$$

Dividing q_x and q_y in Equation (13) by the fracture width yields w , the expressions of the average velocities of the fracturing fluid along the x - and y -directions across the entire fracture width are as follows:

$$\begin{cases} v_{fx} = -\frac{w^2}{12\mu} \frac{\partial p}{\partial x} \\ v_{fy} = -\frac{w^2}{12\mu} \frac{\partial p}{\partial y} \end{cases} \quad (13)$$

The fracturing fluid flow can be described as:

$$\nabla \cdot \left[\frac{w^3(x, y, t)}{12\mu} \nabla p(x, y, t) \right] - 2v_l(x, y, t) = \frac{\partial w(x, y, t)}{\partial t} \quad (14)$$

2.4. Fracture Width Equation

England and Green proposed a relationship between normal stress acting on the fracture surfaces due to any arbitrary distribution within the fracture and the corresponding induced fracture width under plane strain conditions:

$$w(x, y, t) = -16 \frac{1 - \nu^2}{E} \int_{|z|}^l \frac{F(\tau) + yG(\tau)}{\sqrt{\tau^2 - y^2}} \quad (15)$$

In the PKN model, for the fracture tip perpendicular to the fracture length, the shape of the fracture is elliptical, and its fracture width equation is as follows:

$$w(x, y, t) = \frac{(1 - \nu)}{G} (h^2 - 4y^2)^{\frac{1}{2}} (p(x, y, t) - \sigma_h) \quad (16)$$

In Equation (17), the fluid pressure within the fracture changes only with respect to the fracture length and remains constant at the fracture–height interface. However, for hydraulic fracturing fluid flow in horizontally oriented fractures in the vicinity of the wellbore, there is a radial flow region due to the presence of the fracturing fluid. Therefore, the fluid flow becomes two-dimensional in the x – y plane, with pressure gradients in both the x - and y -directions. In this case, to calculate the fracture width using the equation above at any position along the fracture length, we take the average pressure in the fracture–height direction at that location to compute the fracture width, as follows:

$$w = \frac{(1 - \nu)}{G} (h^2 - 4y^2)^{\frac{1}{2}} \left(\frac{\sum_{j=1}^n p(x, y)}{n} - \sigma_h \right) \quad (17)$$

In the equation, w represents the fracture width, m; h is the fracture height, m; ν is the dimensionless Poisson's ratio; G is the shear modulus, MPa; n is the number of units in the fracture–height direction; and σ_h is the minimum horizontal in situ stress, MPa.

2.5. Proppant Continuity Equation

Using the principle of mass conservation, which states that the net mass inflow of proppant into a control volume is equal to the change in mass of proppant within that control volume, the proppant continuity equation is as follows:

$$\frac{\partial(c\rho_p v_{px} w)}{\partial x} + \frac{\partial(c\rho_p v_{py} w)}{\partial y} + \frac{\partial(c\rho_p w)}{\partial t} = 0 \quad (18)$$

In this equation, v_{px} is the horizontal velocity of the proppant, m/s; and v_{py} is the vertical velocity of the proppant.

2.6. Proppant Velocity Equation

Currently, conventional hydraulic fracturing models, when calculating proppant transport, only consider the settling motion of proppant particles within the fracturing fluid and assume that the horizontal transport velocity of proppant is the same as the horizontal flow velocity of the fracturing fluid. In reality, as proppant particles move within the fracture, the fluid velocity within the fracture varies in a parabolic distribution across the fracture width. At the center of the fracture, the shear forces are minimal, and the fracturing fluid velocity is at its maximum, as shown in Figure 4. Proppant particles tend to move toward areas of lower shear forces, i.e., the central region of the fracture. As a result, the horizontal transport velocity of the proppant may be greater than the average fluid velocity. However, during the actual fracturing process, the movement of the proppant within the fracture is also influenced by the fracture surface and proppant concentration, which may lead to the proppant's horizontal transport velocity often being less than the average fluid velocity.

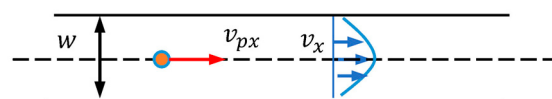


Figure 4. Fracturing fluid velocity profile.

Therefore, in the actual hydraulic fracturing process, there exists both vertical velocity slip and horizontal velocity slip between the proppant and the fracturing fluid. In the second chapter, we provided expressions for the proppant settling velocity and horizontal transport velocity. Thus, the proppant's transport velocity can be expressed as:

$$v_p = v_{px} \cdot \mathbf{i} + v_{py} \cdot \mathbf{j} \quad (19)$$

where

$$\begin{cases} v_{px} = v_{fx} \cdot f_h \\ v_{py} = v_{fy} + v_{s_c} \end{cases} \quad (20)$$

In Equation (20), v_{fx} is the fracturing fluid velocity in the x-direction, m/s; v_{fy} is the fracturing fluid velocity in the y-direction, m/s; f_h is the dimensionless proppant horizontal transport velocity correction factor; and v_{s_c} is the corrected proppant settling velocity, m/s.

$$\begin{aligned} w \frac{\partial c}{\partial t} - (1-c) \frac{\partial w}{\partial t} - \frac{\partial}{\partial x} \left[\left((1-c) + c \frac{\rho_p}{\rho_f} (1-h_f) \right) q_x \right] \\ - \frac{\partial}{\partial x} \left[(1-c) q_y - c v_{s_c} \frac{\rho_p}{\rho_f} \right] = v_l \end{aligned} \quad (21)$$

Once the proppant concentration distribution at various points within the fracture is determined, the viscosity of the slurry can be modified using the following equation. The modified slurry viscosity is then used in place of the fracturing fluid viscosity for the calculation of fracture width and flow field distribution in the subsequent time step.

$$\mu_{slurry} = \mu_f \left(\frac{1-c_p}{1-c_p/c_m} \right)^{\frac{a_1-c_m}{1-c_m}} \quad (22)$$

In this equation, μ_{slurry} represents the viscosity of the slurry, mPa · s; c_p is the viscosity of the fracturing fluid, a dimensionless fraction; a_1 is the volume concentration of the proppant, a dimensionless fraction; c_m is the volume fraction of the proppant when randomly densely packed, a dimensionless fraction; and a_1 is the first-order viscosity coefficient, a dimensionless fraction. Here, we take c_m and a_1 as 0.64 and 2.5, respectively.

2.7. Initial Conditions and Boundary Conditions

By combining equations, we obtain the system of governing equations for solving proppant transport in a horizontally fractured well. To obtain a unique solution, initial conditions and boundary conditions for these equations must be provided.

(1) Initial conditions

At the initial moment, the fracture width is zero, and the proppant concentration within the fracture is zero, i.e.,:

$$\begin{cases} w(x, y, 0) = 0 \\ c(x, y, 0) = 0 \end{cases} \quad (23)$$

(2) Boundary conditions

In the wellbore perforation segment, the flow rate of the fracturing fluid is equal to the injection rate. When the proppant-laden slurry injection begins, the proppant concentration at the perforation location is the same as the proppant concentration in the injected slurry:

$$\begin{cases} -\frac{w^3}{12\mu} \left(\frac{\partial p}{\partial n} \right) \Big|_{\partial\Omega_{perf}} = Q_i \\ c(\partial\Omega_{perf}, t) = c_{inj}; (t \geq t_s) \end{cases} \quad (24)$$

At the leading edge of the fracture and the upper and lower boundaries, the flow rate of the fracturing fluid is zero, and the proppant concentration gradient is zero:

$$\begin{cases} -\frac{w^3}{12\mu} \left(\frac{\partial p}{\partial x} \right) \Big|_{\partial\Omega_{tip}} = 0 \\ -\frac{w^3}{12\mu} \left(\frac{\partial p}{\partial y} \right) \Big|_{\partial\Omega_{bound}} = 0 \\ \frac{\partial c}{\partial x} \Big|_{\partial\Omega_{tip}} = 0 \\ \frac{\partial c}{\partial y} \Big|_{\partial\Omega_{bound}} = 0 \end{cases} \quad (25)$$

Above, by combining the fracture width equation, slurry continuity equation, slurry flow equation, and proppant transport equation with the given initial conditions and boundary conditions, a closed system of governing equations for solving proppant transport is established.

2.8. Numerical Solution

The system of governing equations for hydraulic fracturing fluid flow and proppant transport in horizontally fractured wells, composed of equations, is a system of partial differential equations. These equations are coupled together, making direct analytical solutions difficult; thus, numerical methods are used. By numerically solving the above governing equations, it is possible to obtain the fracture width, fracture internal pressure distribution, fracturing fluid velocity distribution within the fracture, and proppant concentration distribution.

This paper primarily employs the finite difference method. By discretizing the governing equations and initial/boundary conditions, corresponding difference equations are constructed. Then, the computational domain is divided into a grid, and these difference equations are iteratively solved on the grid. Ultimately, this approach yields a numerical solution to the problem.

$$\begin{aligned} & \frac{f_{h_{i+1,j}} q_{x_{i+1,j}} c_{i+1,j} - f_{h_{i-1,j}} q_{x_{i-1,j}} c_{i-1,j}}{2\Delta x} + \frac{(q_{y_{i,j+1}} - v_{s_{-c_{i,j+1}}} w_{i,j+1}) c_{i,j+1}}{2\Delta y} \\ & - \frac{(q_{y_{i,j-1}} - v_{s_{-c_{i,j-1}}} w_{i,j-1}) c_{i,j-1}}{2\Delta y} + \frac{c_{i,j}^{n+1} w_{i,j}^{n+1} - c_{i,j}^n w_{i,j}^n}{\Delta t} = 0 \end{aligned} \quad (26)$$

3. Numerical Simulations

The basic reservoir parameters used for the simulation and construction pumping procedures are shown in Tables 1 and 2, respectively. It is usually considered that the horizontal transportation speed of the proppant is the same as the horizontal flow rate of fracturing fluid, but, in fact, due to the influence of fracture wall and proppant concentration, the horizontal transportation of the proppant is subject to hysteresis, and its horizontal speed is smaller than the horizontal speed of fracturing fluid. Calculations were carried out under the conditions of considering the retardation of the horizontal transport of the proppant and without considering it, and the results are shown in Table 3. It can be seen from the Figure 5 that after considering the retardation of the fracture wall and the concentration of the proppant, the horizontal transport distance of the proppant is clearly reduced, and the length of the proppant slit is also clearly reduced under the same pumping program.

Table 1. The basic parameters of formation.

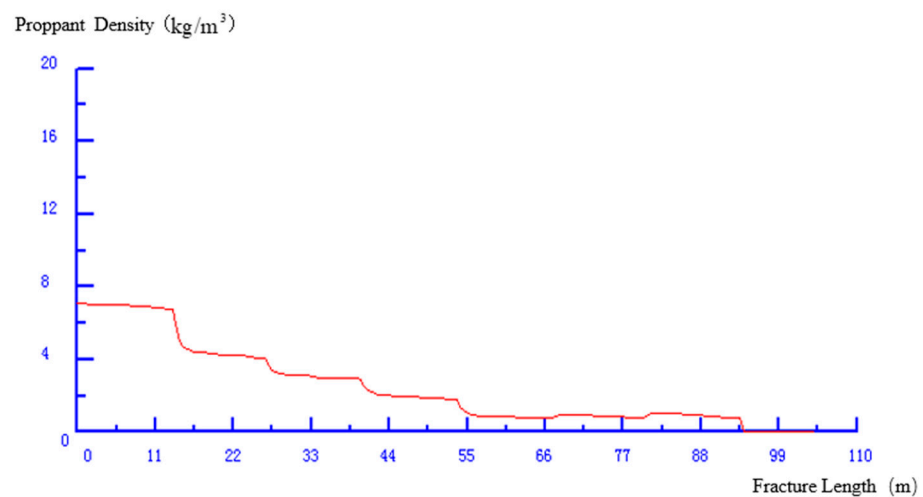
Parameter	Value
Reservoir Thickness/m	25
Elastic Modulus/GPa	30
Poisson's Ratio	0.2
Minimum Horizontal Stress/MPa	35
Formation Permeability/m/min ^{0.5}	0.0008
Proppant Particle Size/Mesh	20/40
Proppant Density/kg/m ³	2500
Proppant Porosity	0.3
Fracturing Fluid Viscosity/mPa·s	1

Table 2. Pumping schedule.

Pumping Stages	Pumping Volume (m ³)	Sand Ratio/%	Discharge (m ³ /min)	Time (min)
1	30	0	3	10
2	20	2	3	6.66
3	20	4	3	6.66
4	20	6	3	6.66
5	20	8	3	6.66
6	10	15	3	3.33
total	120			40

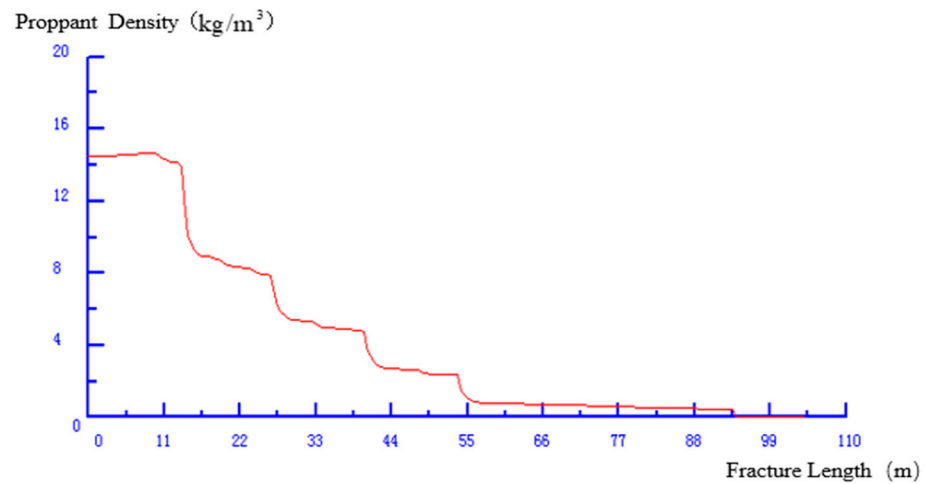
Table 3. Effect of proppant horizontal migration velocity on its distribution.

	Dynamic Fracture Length (m)	Propped Fracture Length (m)	Maximum Proppant Concentration (kg/m ²)	Average Proppant Concentration (kg/m ²)
Neglecting Proppant Horizontal Hindered Settling	105	94	15.06	4.78
Considering Proppant Horizontal Hindered Settling	105	77.5	15.22	5.52

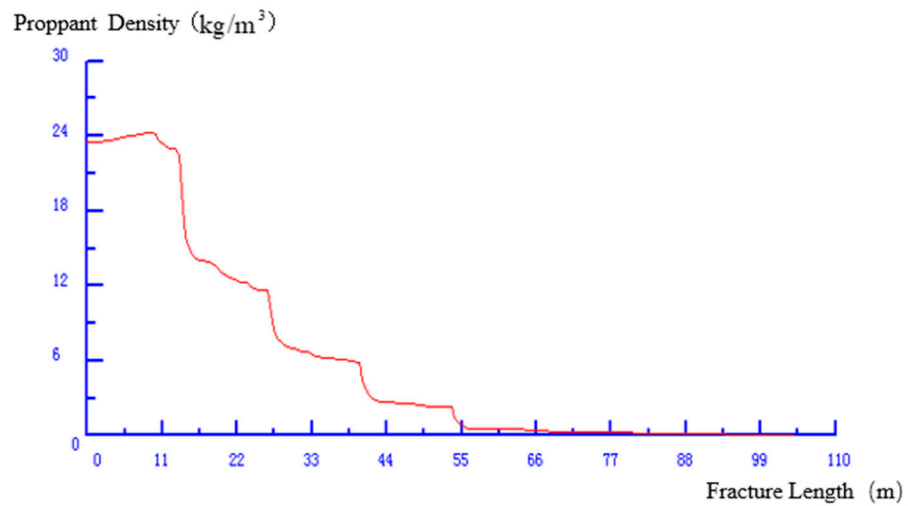


(a) $\rho_p = 1500 \text{ kg/m}^3$

Figure 5. Cont.



$$(b) \rho_p = 2500 \text{ kg/m}^3$$



$$(c) \rho_p = 3500 \text{ kg/m}^3$$

Figure 5. Effect of the proppant density on the distribution of proppant.

3.1. The Impact of Horizontal Transport Velocity on Proppant Distribution

It is usually considered that the horizontal transportation speed of the proppant is the same as the horizontal flow rate of fracturing fluid, but, in fact, due to the influence of the fracture wall and the proppant concentration, the horizontal transportation of the proppant is subject to hysteresis, and its horizontal speed is smaller than the horizontal speed of fracturing fluid. Calculations were carried out under the conditions of considering the retardation of the horizontal transport of the proppant and without considering it, and the results are shown in Table 3. It can be seen from the Figure 5 that after considering the retardation of the fracture wall and the concentration of the proppant, the horizontal transport distance of the proppant is clearly reduced, and the length of the proppant slit is also clearly reduced under the same pumping program.

3.2. The Impact of Proppant Density

The impact of proppant density mainly manifests in the gravity settling of proppant particles. All other conditions being equal, a higher proppant density results in faster settling within the fracture. However, overly rapid settling is not conducive to the transport

of proppant deeper into the fracture. Given the widespread use of low-viscosity fracturing fluids, such as slickwater, in unconventional oil and gas production, proppant settling is a significant concern, as it can severely affect proppant placement and fracturing effectiveness. To address this issue, various ultra-low-density proppants have been developed in recent years. Table 4 and Figure 5 show the results of proppant placement for proppants with densities of 1500, 2650, and 3500. It can be observed that lower-density proppants can achieve longer propped fracture lengths. Although their average proppant concentration is lower, the slow settling in the fracture height direction allows for a larger propped fracture area.

Table 4. Proppant distribution results with different densities.

Proppant Density (kg/m ³)	Dynamic Fracture Length (m)	Propped Fracture Length (m)	Maximum Proppant Concentration (kg/m ²)	Average Proppant Concentration (kg/m ²)
1500	104	95.5	7.08	2.49
2650	104	92.5	14.68	4.32
3500	104	67	24.31	6.19

3.3. The Impact of Proppant Particle Size

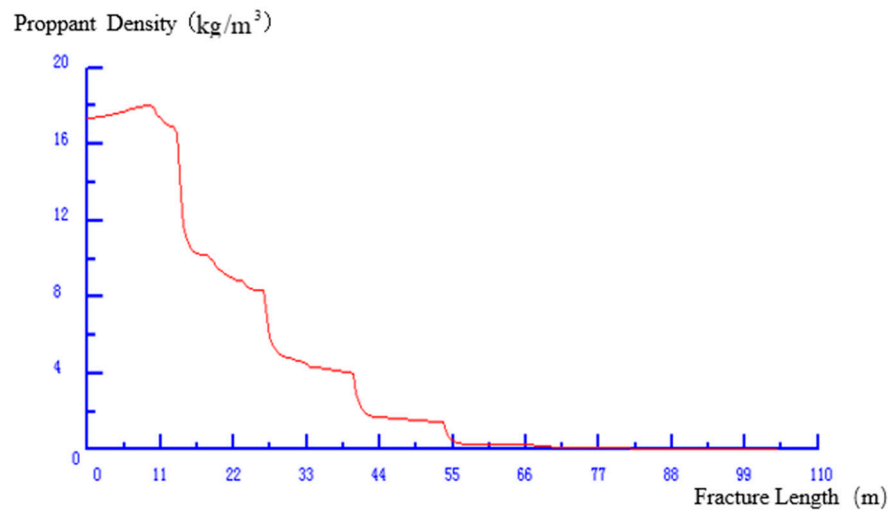
In an infinite free space, larger particle sizes lead to faster settling velocities. However, within an actual fracture, proppant settling is hindered by the fracture walls. Larger proppant particle sizes experience more significant interference and hindrance from the fracture walls. Additionally, the orientation of the fracture walls can also affect the horizontal movement of the proppant. When the ratio of proppant particle size to fracture width is large, it can result in a significant hindrance to the horizontal movement of the proppant. Table 5 and Figure 6 display the placement results for proppants of different mesh sizes. It can be observed that, under the given construction parameters and fracture morphology, the propped fracture length for the 16/30-mesh proppant is much shorter than that for the 20/40-mesh and 40/70-mesh proppants. This is because the larger-particle-sized proppant experiences significant hindrance due to the fracture width. Therefore, in practice, a combination of proppant particle sizes is often used. During the early stages of pumping, smaller proppant sizes are employed to ensure that the fracture tips are supported. In the later stages of pumping, larger proppant sizes can be used to maximize fracture conductivity while maintaining the proppant concentration.

Table 5. Proppant distribution results with different sizes.

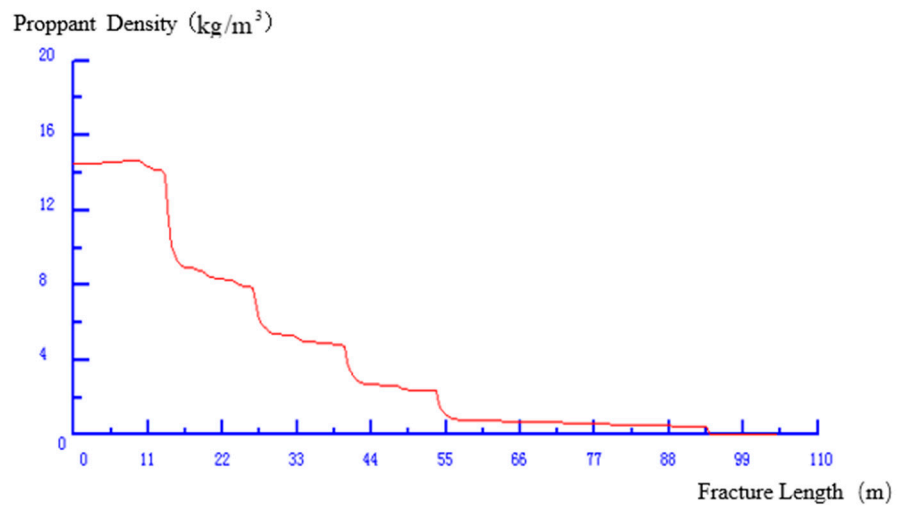
Proppant Mesh Size	Dynamic Fracture Length (m)	Propped Fracture Length (m)	Maximum Proppant Placement (kg/m ²)	Average Proppant Placement Concentration (kg/m ²)
16/30	104	55	18.07	4.46
20/40	104	92.5	14.68	4.32
40/70	104	94	12.97	4.23

3.4. The Impact of Proppant Concentration

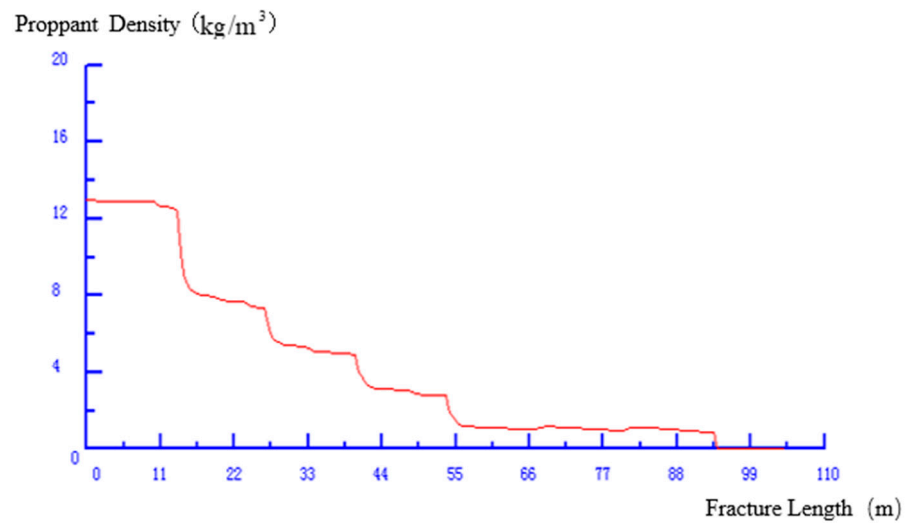
The concentration of the proppant in proppant-laden slurry has a significant impact on the distribution of the proppant within the fracture. Firstly, the proppant concentration interferes with the settling of proppant particles in the fracture, slowing down the settling velocity. It also hinders the horizontal movement of proppant particles within the fracture, thereby reducing the effective propped fracture length. Furthermore, the proppant concentration affects the effective viscosity and rheological properties of the proppant-laden slurry. The effective viscosity of the slurry, in turn, affects the transport of the proppant within the fracture, influencing the concentration distribution of the proppant within the fracture and, ultimately, determining the fracture's conductivity.



(a) 16/30 Mesh size



(b) 20/40 Mesh size



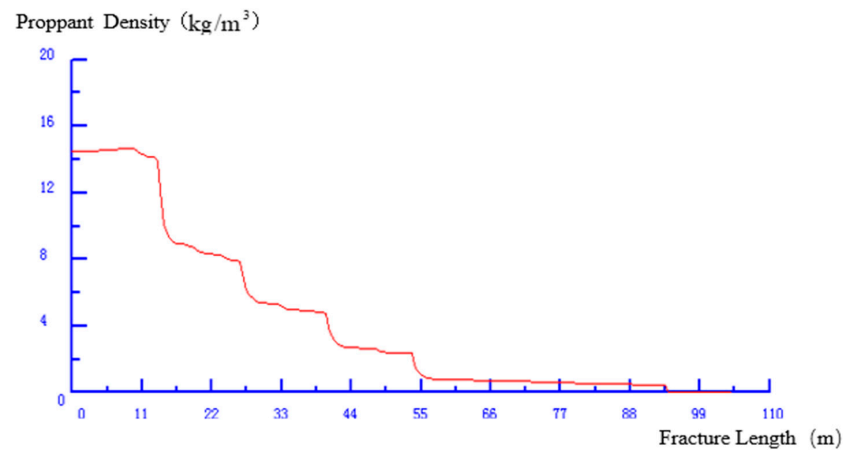
(c) 40/70 Mesh size

Figure 6. Effect of particle size on the distribution of proppant.

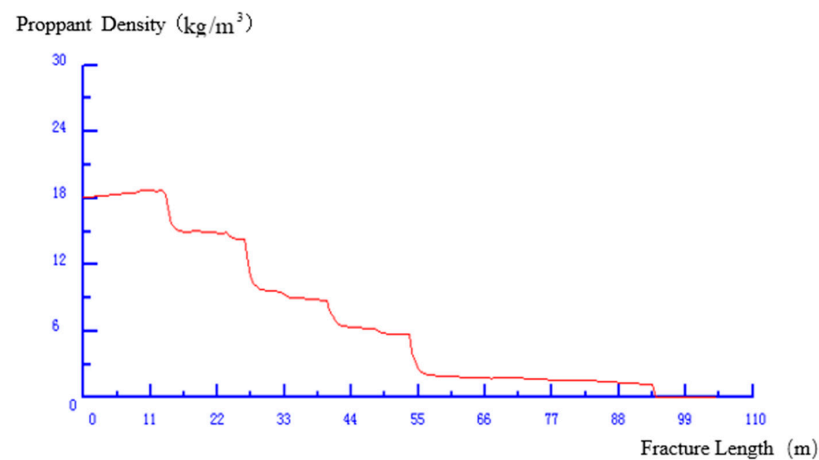
In summary, using different proppant addition programs can affect the distribution of the proppant within the fracture, as well as the post-fracturing conductivity and effective propped fracture area. Improper proppant addition programs can lead to issues, like proppant bridging during the operation or failure to meet the designed fracture conductivity requirements. This study compared the proppant placement status under two different proppant addition programs, as shown in Table 6 and Figure 7. The results indicate that the choice of the proppant addition program has a significant impact on the proppant placement. To prevent proppant bridging, it is advisable to use a lower sand ratio during the early stages of hydraulic fracturing while increasing the sand ratio toward the end of the fracturing process to enhance the conductivity of the fracture near the wellbore.

Table 6. Pumping schedule (2).

Pumping Stages	Pumping Volume (m ³)	Sand Ratio/%	Discharge (m ³ /min)	Time (min)
1	30	0	3	10
2	20	4	3	6.66
3	20	8	3	6.66
4	20	10	3	6.66
5	20	15	3	6.66
6	10	20	3	3.33
Total	120			30



(a)



(b)

Figure 7. Effect of the proppant concentration on the distribution of proppant. (a) Proppant addition program 1. (b) Proppant addition program 2.

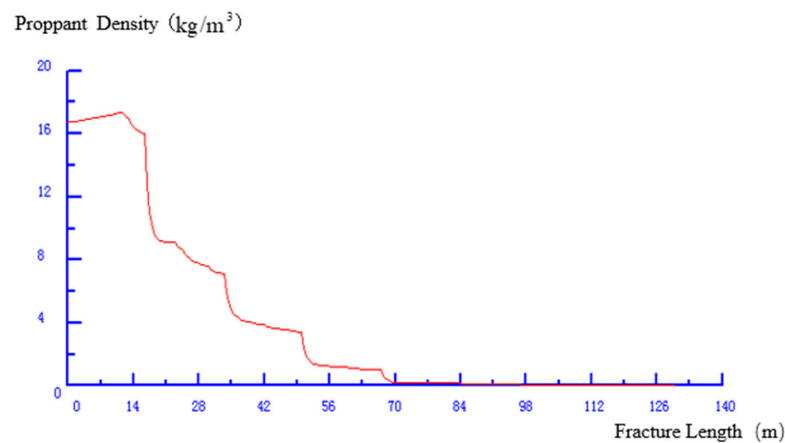
3.5. The Impact of Fracturing Fluid Viscosity

In the hydraulic fracturing process, the viscosity of the fracturing fluid not only influences the geometric shape of the fracture but also plays a crucial role in the transport and placement of the proppant. A higher fracturing fluid viscosity results in increased proppant-carrying capacity and slower proppant settling and is more favorable for transporting the proppant to deeper regions of the fracture. It also leads to greater propped fracture height, thereby obtaining a larger propped fracture area.

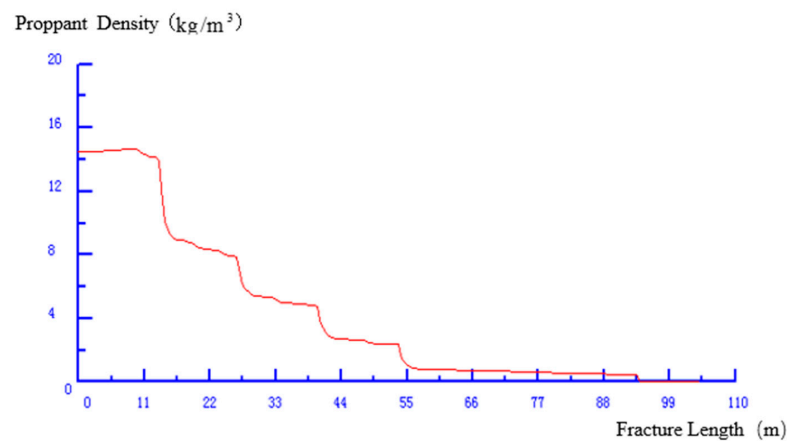
Table 7 and Figure 8 show the proppant placement status under different fracturing fluid viscosities. It can be observed that with increasing viscosity, the proppant concentration near the wellbore decreases, while the proppant concentration in the deeper regions of the fracture increases relatively. This is because high-viscosity fluids can transport more proppant to deeper parts of the fracture. Therefore, during on-site operations, it is advisable to use higher-viscosity fracturing fluids whenever possible, provided that other requirements are met.

Table 7. Proppant distribution results with different fluid viscosities.

Fracturing Fluid Viscosity (1 mPa·s)	Dynamic Fracture Length (m)	Propped Fracture Length (m)	Maximum Proppant Placement Concentration (kg/m ²)	Average Proppant Placement Concentration (kg/m ²)
1	130	68.5	17.35	4.02
10	104	93.5	14.68	4.32
50	86	77.5	13.04	4.42



(a) 1mPa·s



(b) 10mPa·s

Figure 8. Cont.

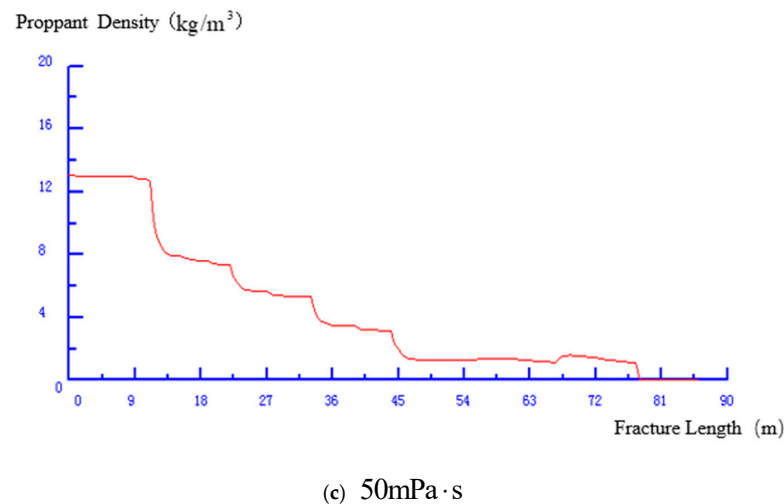


Figure 8. Effect of the fracturing fluid viscosity on the distribution of proppant.

3.6. The Impact of Fracturing Fluid Loss

The rate of fracturing fluid loss is a crucial factor affecting hydraulic fracturing design and execution. Similarly, the magnitude of the fluid loss rate has a significant impact on the transport of the proppant. During the early stages of pumping, slower fluid loss is desirable to facilitate the creation of fractures with the pre-pad fluid. In the later stages of pumping, faster fluid loss is preferred to minimize the closure time of the fracture and ensure the rapid flowback of fracturing fluid into the formation. This reduces the risk of excessive proppant settling and remaining in the producing formation, leading to effective propping.

Table 8 and Figure 9 show the calculated results of the proppant placement status under different fluid loss coefficients. It can be observed that with an increasing fluid loss coefficient, both the dynamic fracture length and propped fracture length decrease. Proppant placement concentration, particularly the maximum proppant placement concentration, increases significantly. Therefore, when the formation has a high fluid loss coefficient, the risk of proppant bridging is significantly higher, and special attention should be paid during the construction process.

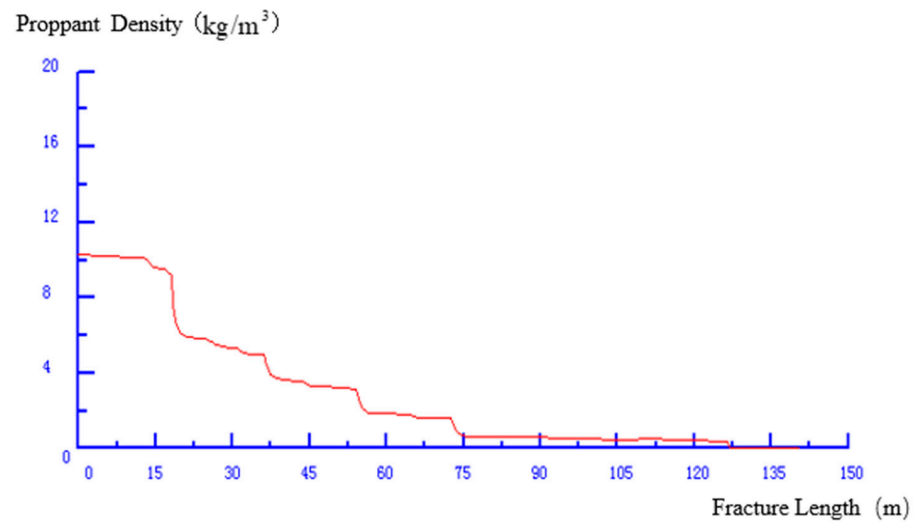
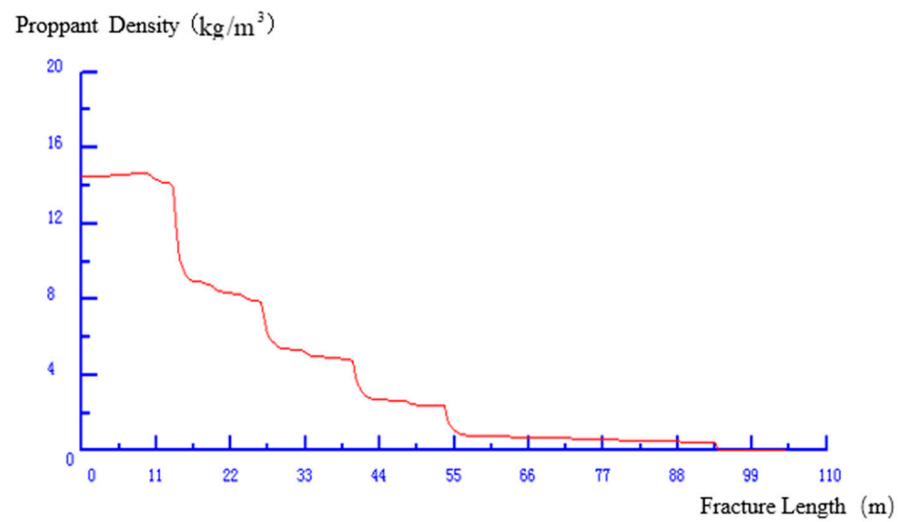
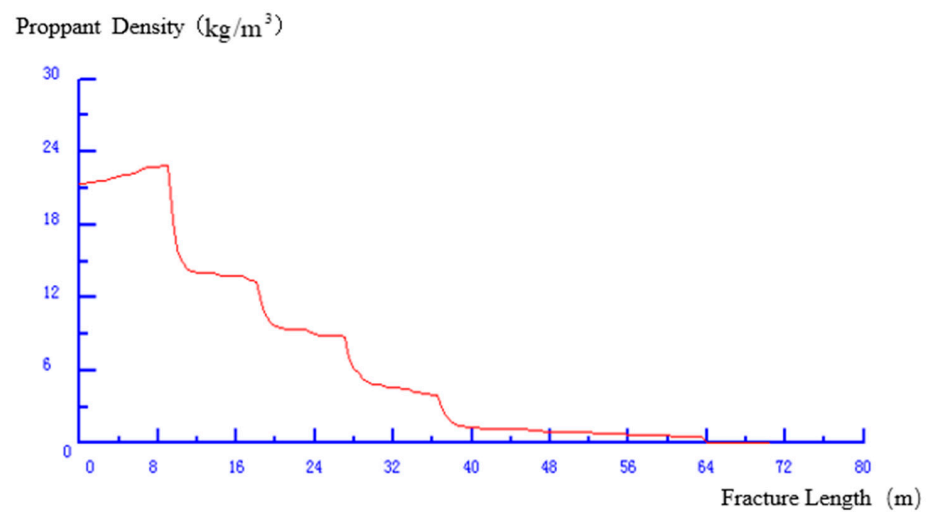
Table 8. Proppant distribution results with different fluid loss coefficients.

Effective Filtration Coefficient (m/√s)	Dynamic Fracture Length (m)	Propped Fracture Length (m)	Maximum Proppant Placement Concentration (kg/m ³)	Average Proppant Placement Concentration (kg/m ³)
0.0002	140.5	126.5	10.29	2.92
0.0004	104	93.5	14.68	4.32
0.0006	70.5	63.5	22.91	7.03

3.7. The Impact of Pumping Rate

The pumping rate is a crucial parameter in hydraulic fracturing, as it not only affects the geometry of the fracture but also has a significant impact on the distribution of the proppant within the fracture. When the pumping rate of the fracturing fluid is low, its carrying capacity is limited, especially for low-viscosity fracturing fluids. In such cases, the proppant quickly settles within the fracture, significantly affecting its horizontal transport distance.

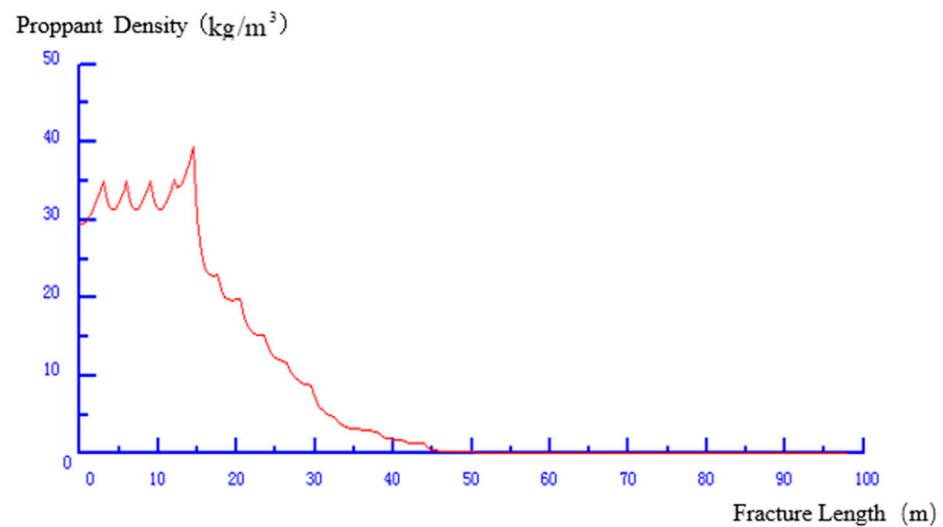
Table 9 and Figure 10 show the results of proppant distribution under different pumping rates. The results indicate that with a smaller pumping rate, the fracture length is also smaller, leading to rapid settling of the proppant near the wellbore, resulting in a high proppant placement concentration in the near-well zone but a shorter effective propped fracture length. As the pumping rate increases, the fracture length also increases, and high pumping rates facilitate the transport of proppant to deeper parts of the fracture, significantly increasing the propped fracture length.

(a) $C_t = 0.0002$ (b) $C_t = 0.0004$ (c) $C_t = 0.0006$ **Figure 9.** Effect of the fracturing fluid loss coefficient on the distribution of proppant.

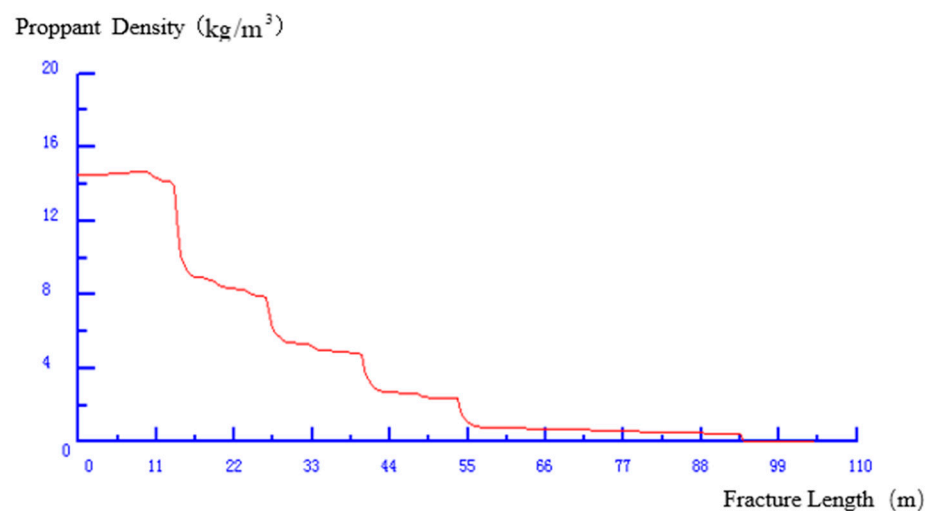
Furthermore, using high pumping rates also helps in forming a complex fracture network structure, further enhancing the effectiveness of hydraulic fracturing. Therefore, during on-site operations, it is advisable to use high pumping rates whenever feasible to achieve both safety and economic goals.

Table 9. Proppant distribution results with different pumping rates.

Discharge Rate (m ³ /min)	Dynamic Fracture Length (m)	Proppant Fracture Length (m)	Maximum Proppant Placement Concentration (kg/m ²)	Average Proppant Placement Concentration (kg/m ²)
1	98	47	39.40	8.05
3	104	93.5	14.68	4.32
5	122	110	15.47	5.27

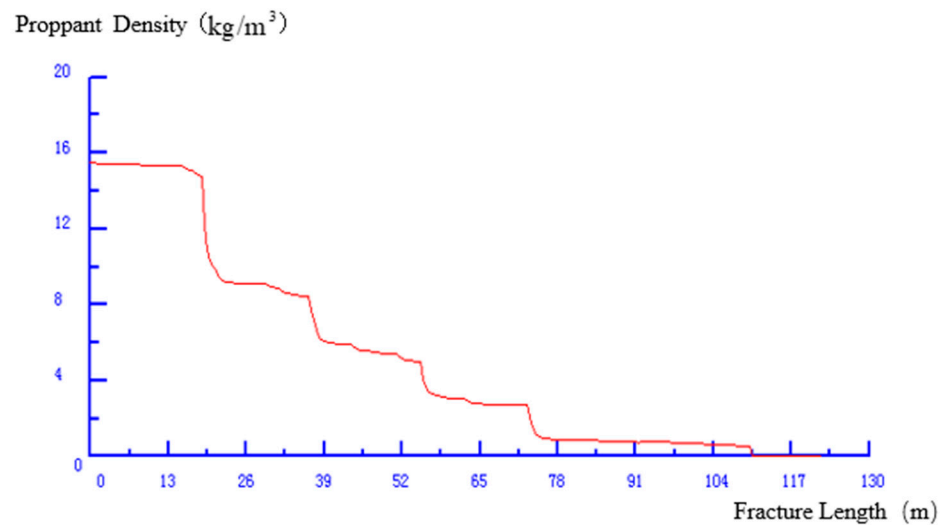


(a) $Q=1\text{m}^3 / \text{min}$



(b) $Q=3\text{m}^3 / \text{min}$

Figure 10. *Cont.*



(c) $Q=3\text{m}^3 / \text{min}$

Figure 10. Effect of pumping rate on the distribution of proppant.

4. Conclusions

(1) During the actual horizontal well fracturing construction process, the fracture initiation and extension, the flow of fracturing fluid in the fracture, and the transportation of the proppant, along with the fracturing fluid in the fracture, is a very complicated process. The model simulated proppant bank creation at the bottom of the fracture during the treatment time. The fracture fills up faster at higher injection rates with less proppant settlement. The viscosity of the carrying fluid has the strongest effect on the amount of proppant settlement. Within practical ranges, parameters such as proppant size and density only have a modest effect on proppant settlement;

(2) The results show that the proppant concentration and the fracture wall effect can slow down the proppant settling speed, but, at the same time, they can also block the horizontal transportation of the proppant and shorten the effective proppant fracture length. Increasing the fracturing fluid viscosity and construction volume, decreasing the proppant density and particle size, and adopting appropriate sand addition procedures can achieve better proppant placement and, thus, better fracturing and remodeling results;

(3) As of now, there is significant uncertainty regarding the effect of the physical proppant and fluid parameters on the final proppant distribution. The numerical model presented here enhances our understanding of the relationship between the fluid and proppant properties and the final proppant distribution that determines the conductivity of the propped fracture. The outcome is the improved design and implementation of the fracpack operation and reduced uncertainty in the fracpack performance.

Author Contributions: Conceptualization, Z.C. and X.X.; methodology, Z.C.; software, G.W.; validation, Z.C., Y.H. and B.G.; formal analysis, X.X.; investigation, Y.X.; resources, Z.C.; data curation, Y.H.; writing—original draft preparation, Z.C.; writing—review and editing, X.X.; visualization, G.W.; supervision, Z.C. and Y.X.; project administration, B.G.; funding acquisition, Z.C. All authors have read and agreed to the published version of the manuscript.

Funding: This research was funded by [Research on offshore large-scale fracturing engineering technology], grant number [KJGG2022-0704], The APC was funded by [Technology Information Department of the Group Company]. The author declare that this study received funding from China National Offshore Oil Corporation, Technology Information Department of the Group Company. The funder had the following involvement with the study: Supervision and Project administration.

Data Availability Statement: The data is all in the paper and no additional data is provided

Conflicts of Interest: Author Zhengrong Chen, Xin Xie, Guangai Wu and Yanan Hou were employed by the company China National Offshore Oil Corporation. The remaining authors declare that the research was conducted in the absence of any commercial or financial relationships that could be construed as a potential conflict of interest.

References

1. Bandara, K.M.A.S.; Ranjith, P.G.; Rathnaweera, T.D.; Wanniarachchi, W.A.M.; Yang, S.Q. Crushing and embedment of proppant packs under cyclic loading: An insight to enhanced unconventional oil/gas recovery. *Geosci. Front* **2021**, *12*, 100970. [[CrossRef](#)]
2. Cohen, C.E.; Abad, C.; Weng, X.; England, K.; Phatak, A.; Kresse, O.; Newonen, O.; Lafitte, V.; Abivin, P. Optimum fluid and proppant selection for hydraulic fracturing in shale gas reservoirs: A parametric study based on fracturing-toproduction simulations. In Proceedings of the SPE Hydraulic Fracturing Technology Conference, The Woodlands, TX, USA, 4 February 2013; Society of Petroleum Engineers: The Woodlands, TX, USA, 2013; pp. 652–669.
3. Shi, F. XFEM-based numerical modeling of well performance considering proppant transport, embedment, crushing and rock creep in shale gas reservoirs. *J. Pet. Sci. Eng.* **2021**, *201*, 108523. [[CrossRef](#)]
4. Hari, S.; Krishna, S.; Gurralla, L.N.; Singh, S.; Ranjan, N.; Vij, R.K.; Shah, S.N. Impact of reservoir, fracturing fluid and proppant characteristics on proppant crushing and embedment in sandstone formations. *J. Nat. Gas Sci. Eng.* **2021**, *95*, 104187. [[CrossRef](#)]
5. Sahai, R.; Miskimins, J.L.; Olson, K.E. Laboratory results of proppant transport in complex fracture systems. In Proceedings of the SPE Hydraulic Fracturing Technology Conference, The Woodlands, TX, USA, 4–6 February 2014; p. SPE-168579-MS.
6. Wang, J.; Zhang, L.; Xu, H.; Yang, K.; Jiang, H. Migration and sedimentation of proppant and its influencing factors in a visual plate fracture model. *Colloids Surf. A Physicochem. Eng. Asp.* **2023**, *679*, 132548. [[CrossRef](#)]
7. Wang, J.; Huang, Y.; Zhou, F.; Liang, X. The influence of proppant breakage, embedding, and particle migration on fracture conductivity. *J. Pet. Sci. Eng.* **2020**, *193*, 107385. [[CrossRef](#)]
8. Suri, Y.; Islam, S.Z.; Hossain, M. Effect of fracture roughness on the hydrodynamics of proppant transport in hydraulic fractures. *J. Nat. Gas Sci. Eng.* **2020**, *80*, 103401. [[CrossRef](#)]
9. Merzoug, A.; Mouedden, N.; Rasouli, V.; Damjanac, B. Simulation of Proppant Placement Efficiency at the Intersection of Induced and Natural Fractures. In Proceedings of the 56th US Rock Mechanics/Geomechanics Symposium, Santa Fe, NM, USA, 26–29 June 2022.
10. Zheng, Y.; Wang, H.; Wang, B.; Kuru, E.; Ni, J.; Huang, H.; Cheremisin, A.; Stanchits, S. Effect of roughness characteristics of hydraulic fractures on the proppant transport using supercritical CO₂. *Geoenergy Sci. Eng.* **2023**, *227*, 211908. [[CrossRef](#)]
11. Akhshik, S.; Rajabi, M. Simulation of proppant transport at intersection of hydraulic fracture and natural fracture of wellbores using CFD-DEM. *Particuology* **2022**, *63*, 112–124. [[CrossRef](#)]
12. Walayat, K.; Wang, Z.; Usman, K.; Liu, M. An efficient multi-grid finite element fictitious boundary method for particulate flows with thermal convection. *Int. J. Heat Mass Transf.* **2018**, *126*, 452–465. [[CrossRef](#)]
13. Barboza, B.R.; Chen, B.; Li, C. A review on proppant transport modelling. *J. Pet. Sci. Eng.* **2021**, *204*, 108753. [[CrossRef](#)]
14. Patankar, N.A.; Joseph, D.D. Modeling and numerical simulation of particulate flows by the Eulerian–Lagrangian approach. *Int. J. Multiphas. Flow* **2001**, *27*, 1659–1684. [[CrossRef](#)]
15. Zhang, G.; Zhang, Y.; Xu, A.; Li, Y. Microflow effects on the hydraulic aperture of single rough fractures. *Adv. Geo-Energy Res.* **2019**, *3*, 104–114. [[CrossRef](#)]
16. Zhou, Y.; Ni, H.; Shen, Z.; Zhao, M. Study on particle settling in supercritical carbon dioxide drilling and fracturing. *J. Pet. Sci. Eng.* **2020**, *190*, 107061. [[CrossRef](#)]
17. Isah, A.; Hiba, M.; Al-Azani, K.; Aljawad, M.S.; Mahmoud, M. A comprehensive review of proppant transport in fractured reservoirs: Experimental, numerical, and field aspects. *J. Nat. Gas Sci. Eng.* **2021**, *88*, 103832. [[CrossRef](#)]
18. Ranjith, P.G.; Wanniarachchi, W.A.M.; Perera, M.S.A.; Rathnaweera, T.D. Investigation of the effect of foam flow rate on foam-based hydraulic fracturing of shale reservoir rocks with natural fractures: An experimental study. *J. Pet. Sci. Eng.* **2018**, *169*, 518–531. [[CrossRef](#)]
19. Gadde, P.B.; Liu, Y.; Norman, J.; Bonnecaze, R.; Sharma, M.M. Modeling proppant settling in water-fracs. In Proceedings of the SPE Annual Technical Conference and Exhibition, Houston, TX, USA, 26–29 September 2004; pp. 373–382.
20. Suri, Y.; Islam, S.Z.; Hossain, M. A new CFD approach for proppant transport in unconventional hydraulic fractures. *J. Nat. Gas Sci. Eng.* **2019**, *70*, 102951. [[CrossRef](#)]
21. Zhang, G.; Gutierrez, M.; Chao, K. Hydrodynamic and mechanical behavior of multi-particle confined between two parallel plates. *Adv. Powder Technol.* **2019**, *30*, 439–450. [[CrossRef](#)]
22. Zhang, B.; Gamage, R.P.; Zhang, C.; Wanniarachchi, A. Hydrocarbon recovery: Optimized CFD-DEM modeling of proppant transport in rough rock fractures. *Fuel* **2022**, *311*, 122560. [[CrossRef](#)]
23. Biheri, G.; Imqam, A. In-Depth Laboratory Proppant Transport Study Using HVFRs for Marcellus High TDS Environments. *SPE J.* **2023**, *28*, 2130–2147. [[CrossRef](#)]
24. Zhao, K.; Wang, J.; Xu, H.; Zhang, L.; Jiang, H. Numerical simulation of proppant migration and sedimentation behavior in complex fractures based on computational fluid dynamics. *Phys. Fluids* **2023**, *35*, 093103. [[CrossRef](#)]

Disclaimer/Publisher’s Note: The statements, opinions and data contained in all publications are solely those of the individual author(s) and contributor(s) and not of MDPI and/or the editor(s). MDPI and/or the editor(s) disclaim responsibility for any injury to people or property resulting from any ideas, methods, instructions or products referred to in the content.